

## Total Transmission and Total Reflection by Zero Index Metamaterials with Defects

Viet Cuong Nguyen,<sup>1</sup> Lang Chen,<sup>1,\*</sup> and Klaus Halterman<sup>2</sup>

<sup>1</sup>*School of Materials Science and Engineering, Nanyang Technological University, 50 Nanyang Avenue, Singapore 639798, Singapore*

<sup>2</sup>*Research and Intelligence Department, Physics Division, Naval Air Warfare Center, China Lake, California 93555, USA*

(Received 6 August 2010; revised manuscript received 30 October 2010; published 3 December 2010)

We theoretically investigate microwave transmission through a zero-index metamaterial loaded with dielectric defects. The metamaterial is impedance matched to free space, with the permittivity and permeability tending towards zero over a given frequency range. By simply varying the radii and permittivities of the defects, total transmission or reflection of the impinging electromagnetic wave can be achieved. The proposed defect structure can offer advances in shielding or cloaking technologies without restricting the object's viewpoint. Active control of the observed exotic transmission and reflection signatures can occur by incorporating tunable refractive index materials such as liquid crystals and BaSrTiO<sub>3</sub>.

DOI: 10.1103/PhysRevLett.105.233908

PACS numbers: 41.20.Jb, 73.20.Mf

The field of metamaterials continues to flourish and evolve, in part due to the recent interest and excitement arising from potential applications involving invisibility cloaking [1,2], perfect lenses [3], and slow light devices [4]. One of the primary thrusts of metamaterials is the design of electromagnetic (EM) structures that have a prescribed response to the incident electric ( $\mathbf{E}$ ) and magnetic ( $\mathbf{H}$ ) fields, characterized by the permittivity  $\epsilon$  and permeability  $\mu$ . The vast number of metamaterials are structures consisting of double negative index media (real parts of  $\epsilon$  and  $\mu$  are negative) [5], single negative index media (real part of  $\epsilon$  or  $\mu$  is negative) [6], epsilon zero media (real part of  $\epsilon$  is zero), and matched impedance zero-index material (MIZIM), where  $\epsilon$  and  $\mu$  both vanish over a narrow frequency window [7,8]. Compared with the double negative index and single negative index materials, zero-index metamaterials (ZIMs), whose permittivity and permeability are simultaneously or individually equal to zero, have received much less attention. As the experimental landscape is continually refined, many of these theoretical concepts once viewed as high risk appear within grasp.

Structures involving ZIMs have been investigated experimentally and theoretically by several scientists [8–16]. The tunneling of EM waves through ultranarrow ZIM channels has been demonstrated experimentally in the rf regime [11,12]. Moreover, a subwavelength ZIM slit can result in strong transmission of EM waves differing from conventional Fabry-Perot resonances [14]. The infrared transmission and reflectivity measurements taken long ago [15] of silicon carbide (SiC) indicated a near-zero index of refraction. The fabrication of metallodielectric ZIMs in the microwave regime was reported [17], and a stacked Drude checkerboard structure was created for IR wavelengths [18]. If the ZIM is impedance matched to free space, where  $\mu$  also vanishes, the corresponding MIZIM can exhibit more dramatic properties. The idea of MIZIM slabs as perfect lenses was discussed [19], and “nihility”

was extended later to scattering by MIZIM cylinders and spheres [20]. It was also shown theoretically that a MIZIM can facilitate total transmission without changing the phase, and act as a transformer that converts small-curvature wave fronts into output beams with planarlike wave fronts [16]. As investigations into the full phenomena that can arise in MIZIMs is still incomplete, there are some limited experimental results, including successful fabrication of a mid-IR MIZIM [21].

Our aim is to reveal how total reflection and total transmission of an EM wave can occur by simply controlling the geometrical and material properties of certain “defects,” consisting of either conventional dielectric rods or low loss high-dielectric materials (like MgCaTiO<sub>3</sub> or BaTiO<sub>3</sub>) arbitrarily embedded in a MIZIM. The irrotational electric and magnetic fields in the MIZIM permits complementary analytical and numerical solutions to Maxwell's equations. Perfect transmission or reflection can be exploited through variations in either the radius  $R$  of the defect, the frequency of the wave, or the constitutive material values of the defects. It is also shown that considerable field enhancement can arise in extreme-dielectric defects. Finally, we discuss a few of the possible applications for our proposed system, including invisibility and perfect shielding.

We consider an EM wave incident from the left into the structure illustrated in Fig. 1. The  $\mathbf{H}$  field is polarized in the  $z$  direction, and the  $\mathbf{E}$  field is  $y$  directed. For simplicity, we consider the fundamental TEM mode [7]. The central MIZIM layer is a Drude-like material with permittivity,  $\epsilon_1 = 1 - \omega_p^2/[\omega(\omega + i\Gamma)]$ , and permeability,  $\mu_1 = 1 - \omega_p^2/[\omega(\omega + i\Gamma)]$ . The plasma frequency is  $\omega_p$ , and  $\Gamma$  is related to the mean free path. The surrounding free space layers correspond to regions 0 and 3. The defects in region 2 that are embedded in MIZIM consist of  $N$  cylinders with the permittivity and permeability of the  $i$ th cylinder ( $i = 1, 2, 3, \dots, N$ ) equal to  $\epsilon_{2,i}$  and  $\mu_{2,i}$ , respectively. We assume an  $\exp(-i\omega t)$  time dependence throughout, where

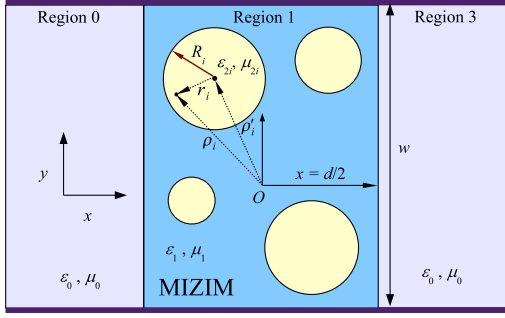


FIG. 1 (color online). Schematic of the proposed vacuum-MIZIM-vacuum metamaterial structure containing an arbitrary arrangement of  $N$  defects (region 2). The propagation direction of the EM wave is along the  $x$  axis. The central MIZIM layer (with  $\epsilon_1$  and  $\mu_1$ ) in region 1 has thickness  $d$  in the  $x$  direction and width  $w$  in the  $y$  direction. The  $i$ th cylindrical defect has radius  $R_i$ , permittivity  $\epsilon_{2,i}$ , and permeability  $\mu_{2,i}$ . The upper and lower boundaries correspond to a perfectly conducting metal or perfect magnetic boundary, depending on the polarization of the incident wave.

$\omega$  is the usual angular frequency. The EM wave in each region must satisfy the Ampère-Maxwell equation,

$$\mathbf{E}_m = \frac{ic}{\omega \epsilon_m} \nabla \times \mathbf{H}_m, \quad (1)$$

where  $c$  is the speed of light in vacuum and the integer  $m$  denotes the region. If we consider the MIZIM region for frequencies near  $\omega_p$ , so that  $\text{Re}[\epsilon_1]$  tends to zero (we take  $\Gamma = 0$  for now),  $\nabla \times \mathbf{H}_1$  must vanish in order to keep the electric field finite [10], resulting in a quasistatic situation. For our  $z$  invariant geometry and incident polarization state, this implies that  $\nabla H_1^z = 0$ , or  $H_1^z$  is a constant, which we denote by  $H_1$ . Because of this condition, any EM scattering from region 2 will result in a net global shift in the magnetic field of region 1 rather than any local spatial fluctuations. For our configuration, Maxwell's equations demand that the EM field in each region must also obey the vector Helmholtz equation,

$$\left( \frac{\partial^2}{\partial x^2} + \frac{\partial^2}{\partial y^2} + \frac{\omega^2}{c^2} \epsilon_m \mu_m \right) \Psi_m = 0, \quad (2)$$

where  $\Psi_m \equiv (\mathbf{E}_m, \mathbf{H}_m)$ . In the limit of  $\epsilon_m$  or  $\mu_m$  vanishing, the Helmholtz equation reduces to the Laplace equation, where quasistatic methods can be utilized. In general, we write  $\mathbf{H}_m = \hat{\mathbf{z}} H_m^z(x, y)$ , and the electric field as  $\mathbf{E}_m = \hat{\mathbf{x}} E_m^x(x, y) + \hat{\mathbf{y}} E_m^y(x, y)$ . For the case of plane wave incidence at oblique angles, the use of a ZIM slab as an angular filter has been discussed [7]. In region 0 the  $\mathbf{H}$  field is the sum of incident and reflected waves that satisfy (2)

$$\mathbf{H}_0 = \hat{\mathbf{z}} H_0 [e^{ik_0(x+d/2)} + \mathcal{R} e^{-ik_0(x+d/2)}], \quad (3)$$

and from (1), the corresponding electric field is

$$\mathbf{E}_0 = \hat{\mathbf{y}} H_0 [e^{ik_0(x+d/2)} - \mathcal{R} e^{-ik_0(x+d/2)}], \quad (4)$$

where  $\mathcal{R}$  is the reflection coefficient,  $k_0$  is the wave vector of free space ( $k_0 = \omega/c$ ), and  $H_0$  is a constant coefficient representing the incident field amplitude.

Similarly, in region 3, the magnetic field is written as  $\mathbf{H}_3 = \hat{\mathbf{z}} H_0 \mathcal{T} \exp(ik_0[x - d/2])$ , with corresponding electric field  $\mathbf{E}_3 = \hat{\mathbf{y}} H_0 \mathcal{T} \exp(ik_0[x - d/2])$ , and where  $\mathcal{T}$  is the transmission coefficient. Equating the tangential components of the EM field at the vacuum-MIZIM interfaces ( $x = -d/2$  and  $x = d/2$ ) reveals a simple relationship between the magnetic field coefficients:  $(\mathcal{R} + 1)H_0 = H_1$  and  $\mathcal{T}H_0 = H_1$ . For a given arrangement of (nonoverlapping) cylindrical defects in the MIZIM, complicated magnetic coupling is avoided, thus permitting a closed form solution to Eq. (2). After implementing Dirichlet boundary conditions at the surface of each defect, we obtain the magnetic field distribution within all  $N$  defects,

$$\mathbf{H}_2 = H_1 \sum_{i=1}^N \frac{J_0(k_{2,i} r_i)}{J_0(k_{2,i} R_i)} \hat{\mathbf{z}}, \quad (5)$$

where  $J_n$  is the Bessel function of the first kind and order  $n$ , and the wave vector in the  $i$ th cylinder  $k_{2,i}$  satisfies the dispersion relation,  $k_{2,i} \equiv k_0 \sqrt{\epsilon_{2,i} \mu_{2,i}}$ . The relative coordinate  $r_i$  conveniently describes points within each defect via  $r_i = |\boldsymbol{\rho}_i - \boldsymbol{\rho}'_i| = \sqrt{(x_i - x'_i)^2 + (y_i - y'_i)^2}$ , where  $x'_i$  and  $y'_i$  locate the centers of each cylinder relative to the prescribed origin of coordinates (see Fig. 1). The sum implies the domain is restricted to the defects. It is straightforward to calculate the electric field inside the defects using Eqs. (5) and (1):

$$\mathbf{E}_2 = iH_1 \sum_{i=1}^N \sqrt{\frac{\mu_{2,i}}{\epsilon_{2,i}}} \frac{J_1(k_{2,i} r_i)}{J_0(k_{2,i} R_i)} \hat{\boldsymbol{\phi}}_i, \quad (6)$$

where  $\hat{\boldsymbol{\phi}}_i$  is the azimuthal unit vector for the  $i$ th cylinder.

To conveniently determine the transmission features, in the MIZIM without intricate details of the electric field in that region, we employ the Faraday-Maxwell equation,  $\mathbf{H}_m = c/(i\omega \mu_m) \nabla \times \mathbf{E}_m$ . It is evident from this expression that as  $\epsilon_1$  and  $\mu_1$  tend to zero,  $\mathbf{E}_1$  becomes irrotational. Subdividing the multiply connected MIZIM region via the appropriate cuts, and applying Stokes' theorem (integration along infinitesimally close cuts cancel), gives the conservation requirement,  $\oint_{\partial C} \mathbf{E} \cdot d\mathbf{l} + \sum_{i=1}^N \oint_{\partial C_{2,i}} \mathbf{E}_{2,i} \cdot d\mathbf{l}_i = 0$ , where  $\partial C$  is the boundary enclosing the whole MIZIM region. After calculating the first line integral above, we have for the transmission coefficient,

$$\mathcal{T} = \frac{1}{1 - (1/2wH_1) \sum_{i=1}^N \oint_{\partial C_{2,i}} \mathbf{E}_{2,i} \cdot d\mathbf{l}_i}, \quad (7)$$

where  $\partial C_{2,i}$  denotes the boundary of each defect. Inserting the  $\mathbf{E}$  field (6) gives

$$\mathcal{T} = \frac{1}{1 - (i\pi/w) \sum_{i=1}^N \sqrt{\mu_{2,i}/\epsilon_{2,i}} [R_i J_1(k_{2,i} R_i)/J_0(k_{2,i} R_i)]}. \quad (8)$$

According to Eq. (8), strong reflection of the incident wave arises if the sum in the denominator diverges (so that  $\mathcal{T} \rightarrow 0$ ). In fact, this can occur if only a *single* defect satisfies  $J_0(k_{2,i} R_i) = 0$ , regardless of the number of other

defects or their material properties,  $\epsilon_{2,i}$  and  $\mu_{2,i}$ . To highlight this phenomenon further, consider Eq. (5), with  $k_{2,i}R_i$  chosen such that denominator of (5) is zero. Then on physical grounds, the magnetic field inside region 1 must vanish to maintain a finite value for  $\mathbf{H}_2$ . Because the  $\mathbf{H}$  field in region 1 is zero, the EM wave is totally reflected, or  $\mathcal{R} = -1$  [see expression above Eq. (5)]. Thus, one can optimize the system for the many combinations of frequency, defect size, and  $\epsilon_{2,i}$  and  $\mu_{2,i}$  that yield zeros to  $J_0(k_{2,i}R_i)$ . A key aspect is that the  $\mathbf{E}$  and  $\mathbf{H}$  fields in the defects are finite. It may be possible to also obtain perfect reflection by coating a cylinder with perfectly magnetic conducting layers [22], but at the cost of eliminating the internal defect field.

The denominator in Eq. (8) also reveals how to achieve perfect transmission of EM energy through the structure. By choosing suitable combinations of  $k_{2,i}$  and  $R_i$  that yield roots to  $J_1(k_{2,i}R_i) = 0$  (for all  $i$ ),  $\mathbf{E}_1$  at the boundary between regions 1 and 2 will also be zero. Each term in the summation in Eq. (8) therefore vanishes and perfect transmission ensues. This criteria also ensures that the perfect transmission phenomenon is insensitive to the width  $d$  of the MIZIM [see Eq. (8)]. This differs from a single ZIM slab, where the transmission varies inversely with the electrical size of the slab [7].

We now complement our analytical results with numerical simulations from a commercial finite element software package [23]. In what follows we take the spatial domain to have dimensions  $w = 44$  mm and  $d = 60$  mm (for the cases studied here, the results are relatively insensitive to these values). Unless otherwise stated, the excitation source has a frequency of  $f = 15$  GHz and all defects are nonmagnetic ( $\mu_{2,i} = 1$ ). Our investigation first centers around the MIZIM region containing three arbitrarily arranged dielectric defects, each with the proper radii and material parameters to yield perfect reflection. In Fig. 2(a), the magnetic field distribution is shown for defects with radii  $R_1 = 4$  mm,  $R_2 = 8$  mm, and  $R_3 = 12$  mm. The corresponding permittivities are  $\epsilon_{2,1} = 3.66$ ,  $\epsilon_{2,2} = 11.86$ , and  $\epsilon_{2,3} = 15.67$ . The plot clearly demonstrates complete reflection of the incident radiation, despite the impedance matching; an unexpected result that holds for even electrically small subwavelength defects ( $R_i/\lambda_0 \ll 1$ ). This is evident by considering the first zero of the Bessel function for a single defect ( $i = 1$ ):  $R/\lambda_0 \approx 0.38274/\sqrt{\epsilon_{2,1}\mu_{2,1}}$ . In Fig. 2(b), the  $\mathbf{E}$  field is shown for the same parameters in 2(a). Although both the  $\mathbf{E}$  and  $\mathbf{H}$  field are curl-free in the MIZIM, the electric field exhibits more complicated behavior, since its 2D polarization state can vary in  $x$  and  $y$ . As alluded to above, if only one defect is tailored to satisfy  $J_0(2\pi\sqrt{\epsilon_{2,i}\mu_{2,i}}R_i/\lambda_0) = 0$  (no matter how electrically small), the other two defects can have arbitrary geometric and material composition without destroying perfect reflectivity. This surprising outcome does not depend on the relative location of a given set of defects due to the quasi-static nature of the EM field in the long wavelength limit.

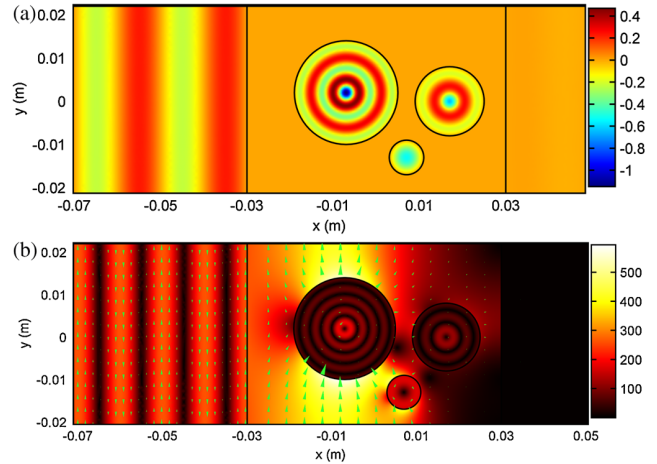


FIG. 2 (color online). Perfect reflection. (a) The magnetic field distribution for an arrangement of three defects embedded in a MIZIM. The radii are  $R_1 = 4$  mm,  $R_2 = 8$  mm, and  $R_3 = 12$  mm with respective materials  $\epsilon_{2,1} = 3.7$ ,  $\epsilon_{2,2} = 11.9$ , and  $\epsilon_{2,3} = 15.7$ . The  $\mathbf{E}$  field magnitude is shown in (b) with its associated vector field distribution (higher field values in the MIZIM occasionally result in some vectors overlapping with an adjacent defect).

In contrast, we now consider the same type of MIZIM and defect configuration to illustrate how incoming waves can undergo complete transmission. In Fig. 3(a), the  $z$  component of the magnetic field is shown as a function of position throughout the structure. The parameters are the same as previously, with only  $\epsilon_{2,i}$  adjusted to satisfy vanishing of the sum in Eq. (8). The magnetic field is of course uniform in the MIZIM with standing Bessel waves in the defects. Figure 3(b) is the corresponding  $\mathbf{E}$  field with its vector field distribution. The electric field plot shows that after the incident wave penetrates the metamaterial, it immediately becomes distorted in a nontrivial fashion. Moreover, the  $\mathbf{E}$  field in the defects is oriented purely in the  $\hat{\phi}$  direction [see also Eq. (6)], vanishes at the boundary, and then abruptly transitions to a radial field. Just as in Fig. 2(b), the  $\mathbf{E}$  field among defects exhibits a complicated spatial dependence. In Fig. 3(c), the magnitude of the (time-averaged) Poynting vector,  $\mathbf{S} = c/(8\pi) \text{Re}[\mathbf{E} \times \mathbf{H}^*]$ , is shown with vector field overlays. The energy flow tends to “wrap around” the defects, and is compensated by higher energy flux in regions exterior to the defects to satisfy energy conservation. In all, Figs. 3(a)–3(c) demonstrate the incident wave emerging from the MIZIM or defect structure in its original form. This type of structure can thus provide an alternative cloaking scenario that does not involve distorting the EM field via transformation media [24]. It also differs from the mechanism behind scattering cancellation [2]. The underlying physics resides in the long phase variation and “tunneling” effect [10] inherent to near-zero index materials. The defect’s EM signatures of the impinging source wave may also serve as a type of sensor, serving as an “observation window” into the surroundings as mentioned in other contexts [2,25].

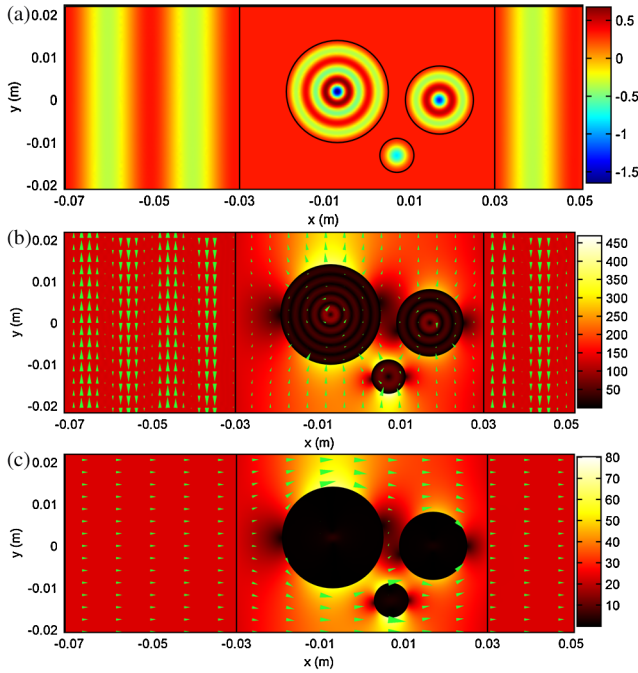


FIG. 3 (color online). Various field profiles illustrating perfect transmission. In (a) the magnetic field pattern is shown for the same setup as Fig. 2 but with the modifications  $\epsilon_{2,1} = 9.3$ ,  $\epsilon_{2,2} = 16.4$ , and  $\epsilon_{2,3} = 19.1$ . In (b) the corresponding  $\mathbf{E}$  field is shown (higher field values in the MIZIM occasionally result in some vectors overlapping with an adjacent defect). The power flow is illustrated in (c) with the Poynting vector map (time averaged over one period) and filled contours representing its magnitude.

The transmitted power as a function of the rod geometry or electrical response can yield further insight into the role that defects play in transmissivity and reflectivity enhancement crucial in the cloaking or shielding of an object. In Fig. 4(a), the transmission ( $S_{21}$ ) is plotted as a function of

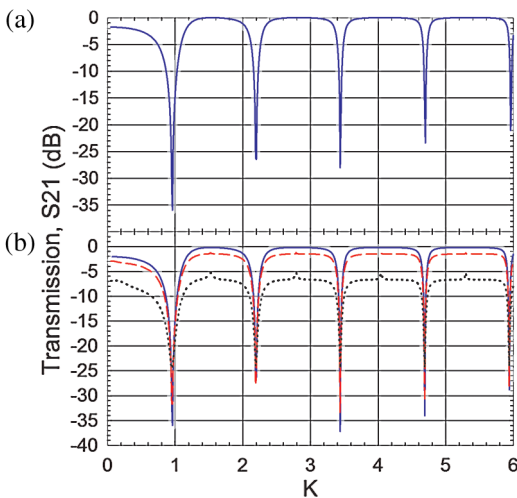


FIG. 4 (color online). (a) Transmission ( $S_{21}$ ) versus  $K$  (see text) of the 8 mm defect for the three defect system in Fig. 3. The effects of loss are shown in (b) for  $\Gamma/\omega_p = 0.001$  (solid line), 0.01 (dashed line), and 0.05 (dotted line).

the material parameter  $K$ , where  $K \equiv \sqrt{\epsilon_{2,2}}$ . Similar results follow for variations in the defect radius. Without loss of generality, we vary only the intermediate sized defect (8 mm). The transmission peaks coincide with the corresponding Bessel function zeros, i.e., when  $J_1(k_{2,i}R_i) = 0$ . Likewise, reflection dips occur where  $J_0(k_{2,i}R_i)$  vanishes (as does the magnetic field in the MIZIM). Not surprisingly, incorporating a small amount of loss reduces the effect somewhat without shifting the location of the peaks [Fig. 4(b)]. The close proximity of the maxima and minima in the transmission spectra might be accessible via active tuning of the defects in real time through inclusion of liquid crystals or BaSrTiO<sub>3</sub>, creating a potential host of reconfigurable devices [26]. For shielding technologies, subwavelength defect cavities can contain elements that have the effective material parameters necessary for perfect reflection.

L. C. acknowledges support from NTU. K. H. is supported in part by ONR and by a grant of HPC resources as part of the DOD HPCMP and would like to thank J. Martin for useful discussions.

\*langchen@ntu.edu.sg

- [1] D. Schurig *et al.*, *Science* **314**, 977 (2006).
- [2] A. Alú and N. Engheta, *Phys. Rev. Lett.* **102**, 233901 (2009).
- [3] J. B. Pendry, *Phys. Rev. Lett.* **85**, 3966 (2000).
- [4] L. V. Alekseyev and E. Narimanov, *Opt. Express* **14**, 11184 (2006).
- [5] V. G. Veselago, *Sov. Phys. Usp.* **10**, 509 (1968).
- [6] H.-K. Yuan *et al.*, *Opt. Express* **15**, 1076 (2007).
- [7] A. Alú *et al.*, *Phys. Rev. B* **75**, 155410 (2007).
- [8] M. Silveirinha and N. Engheta, *Phys. Rev. B* **75**, 075119 (2007).
- [9] R. J. Pollard *et al.*, *Phys. Rev. Lett.* **102**, 127405 (2009).
- [10] M. Silveirinha and N. Engheta, *Phys. Rev. Lett.* **97**, 157403 (2006).
- [11] Ruopeng Liu *et al.*, *Phys. Rev. Lett.* **100**, 023903 (2008).
- [12] B. Edwards *et al.*, *Phys. Rev. Lett.* **100**, 033903 (2008).
- [13] B. Edwards *et al.*, *J. Appl. Phys.* **105**, 044905 (2009).
- [14] K. Halterman and S. Feng, *Phys. Rev. A* **78**, 021805 (2008).
- [15] W. G. Spitzer *et al.*, *Phys. Rev.* **113**, 127 (1959).
- [16] R. W. Ziolkowski, *Phys. Rev. E* **70**, 046608 (2004).
- [17] M. A. Gingrich and D. H. Werner, *Electron. Lett.* **41**, 1266 (2005).
- [18] D.-H. Kwon *et al.*, *Electron. Lett.* **43**, 319 (2007).
- [19] A. Lakhtakia, *Int. J. Infrared Millim. Waves* **23**, 339 (2002).
- [20] A. Lakhtakia, *Microw. Opt. Technol. Lett.* **48**, 895 (2006).
- [21] Z. Jiang *et al.*, in *Proceedings of the Antennas and Propagation Society International Symposium, Charleston, SC, 2009* (IEEE, New York, 2009).
- [22] J. Hao, W. Yan, and M. Qiu, *Appl. Phys. Lett.* **96**, 101109 (2010).
- [23] COMSOL Multiphysics, <http://www.comsol.com>.
- [24] J. Li and J. B. Pendry *Phys. Rev. Lett.* **101**, 203901 (2008).
- [25] G. Castaldi *et al.*, *Opt. Express* **17**, 3101 (2009).
- [26] D. H. Werner *et al.*, *Opt. Express* **15**, 3342 (2007).